Japanese Journal of Applied Physics **53**, 07KF21 (2014) **REGULAR PAPER**
http://dx.doi.org/10.7567/JJAP.53.07KF21

Improvement of myocardial displacement estimation using subkernels for cross correlation between ultrasonic RF echoes

Dai Asari[1], Hideyuki Hasegawa[2,1], and Hiroshi Kanai[1,2*]

[1]*Graduate School of Engineering, Tohoku University, Sendai 980-8579, Japan*
[2]*Graduate School of Biomedical Engineering, Tohoku University, Sendai 980-8579, Japan*
E-mail: kanai@ecei.tohoku.ac.jp

Received November 29, 2013; accepted March 30, 2014; published online June 24, 2014

Speckle tracking is a useful diagnostic method for assessing the cardiac function from ultrasonic echoes. Some factors influence the performance of the conventional speckle tracking method. Deformation due to myocardial contraction and relaxation decreases the correlation between RF echoes. Also, if a strong echo, such as echoes from the epicardium, is included in a correlation kernel, the displacement estimated from the kernel becomes close to the displacement of the epicardium even when the myocardium in the middle of the heart wall is the target to be tracked. To overcome such a problem, in the present study, we proposed a two-step tracking method. In the first step, the displacement is coarsely estimated using a correlation kernel of size similar to that in conventional speckle tracking of (13.8°, 9.1 mm) in the lateral and axial directions. The kernel is divided into small subkernels (2.8°, 1.9 mm). By estimating the correlation coefficient with respect to each subkernel and averaging correlation coefficients obtained from all subkernels, the contribution of a peculiar strong echo included in one of the subkernels can be suppressed. In the second step, the residual displacement is finely estimated using a smaller kernel (13.8°, 3.6 mm). Using a smaller kernel, the influence of myocardial deformation can be suppressed, but there might be multiple regions that have echo patterns similar to that in the kernel, leading to tracking errors. Therefore, the search region in the second step is narrowed because the coarse displacement has already been estimated and compensated in the first step. In the present study, the proposed method was validated using a phantom made of urethane rubber, which was deformed by an actuator. The displacement of the phantom could be estimated with a lower error of 0.059 mm by the proposed method compared to the error in the conventional method of 0.097 mm. Furthermore, the proposed method was applied to in vivo measurement of the human heart. The myocardial displacement could be estimated successfully even when the epicardium was included in a correlation kernel. These results show that the proposed method provides a more accurate and robust estimation of the myocardial displacement.

1. Introduction

Circulatory diseases are increasing due to the westernization of diet, lack of exercise, and aging of society. Therefore, early detection of such diseases is very important. Ultrasonic diagnosis is noninvasive to the human body and cost effective. Therefore, diagnostic ultrasound is widely used for diagnosis of the circulatory system, such as arteries[1–10] and the heart.[11–16] Although the morphological information obtained using ultrasonic diagnostic equipment is useful, functional imaging of tissues would provide beneficial diagnostic information.[17–23] Particularly in echocardiography, myocardial strain and strain rate have also been shown to be effective in the diagnosis of myocardial function.[22,24–27] For the assessment of myocardial motion and deformation, the speckle tracking method,[28–31] which estimates motion using backscattered ultrasonic echoes by regional pattern-matching techniques,[32] is widely used.

However, in a conventional speckle tracking algorithm, myocardial deformation caused by contraction and relaxation often degrades the accuracy of displacement estimation.[33,34] In the calculation of the cross-correlation function between ultrasonic RF echoes, motion accompanied by the deformation of cardiac muscle (not only parallel motion) decreases the correlation between RF signals and leads to an estimation error. Also, if a strong echo, such as an echo from the epicardium, is included in a correlation kernel, the displacement estimated from the kernel becomes close to the displacement of the epicardium even when the displacement of the myocardium in the middle of the heart wall, which is located at the center of the kernel, is desired to be estimated.

To overcome the above problems, in the present study, we employed a two-step tracking method.[35–38] In the first step, the motion of a target point is coarsely estimated. During this process, in the present study, the kernel was divided into small subkernels to suppress the influence of a peculiar strong echo. Then, the residual small displacement was finely estimated in the second step using a smaller correlation kernel to reduce the influence of the myocardial deformation. The novelty of this method is application of the divided kernel to suppress the influence of strong echo. In the present study, the proposed approach was validated by a basic experiment using a silicone phantom deformed by an actuator. Also, we conducted an in vivo measurement of a human heart to show the feasibility of the proposed method.

2. Principles

2.1 First step: Coarse estimation with divided kernel

In the present study, myocardial two-dimensional (2D) displacement was estimated by speckle tracking using the normalized cross-correlation function between ultrasonic RF echoes. In the first step, a larger kernel in the lateral and axial directions, whose central position was $\mathbf{p}_1$, was used for coarse displacement estimation. Typically, a larger kernel is desirable to increase the uniqueness of speckle patterns, thus a larger kernel in general realizes a more robust displacement estimation at the expense of the spatial resolution.[33,39,40] In this step, to suppress the influence of a peculiar strong echo, the larger kernel is divided into 5×5 blocks (subkernels).

With respect to the lag $\delta\mathbf{p} = (\delta\theta, \delta z)$ between kernels in two frames, the normalized correlation function $\gamma_{ij}(\delta\theta, \delta z)$ $(i = -2, -1, \ldots, 2; j = -2, -1, \ldots, 2)$ was obtained for each subkernel. By averaging correlation functions $\{\gamma_{ij}(\delta\theta, \delta z)\}$ of all subkernels, contributions of subkernels are equalized even when a subkernel contains a peculiar strong echo. The total correlation function $\gamma(\delta\theta, \delta z)$ is defined by

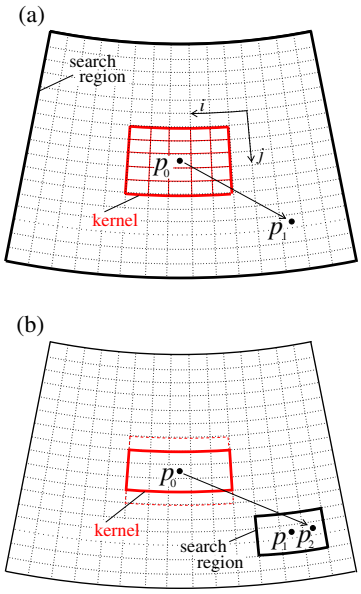

Fig. 1. (Color online) Illustration of displacement estimation by the proposed method. (a) First step using divided subkernels. (b) Second step using a smaller kernel.

$$\gamma(\delta\theta, \delta z) = \frac{\sum_{i=-2}^{2}\sum_{j=-2}^{2} w_{ij}\gamma_{ij}(\delta\theta, \delta z)}{\sum_{i=-2}^{2}\sum_{j=-2}^{2} w_{ij}}, \quad (1)$$

$$w_{ij} = \frac{1}{2\pi\sigma^2}\exp\left\{-\frac{1}{2\sigma^2}(i^2 + j^2)\right\}, \quad (2)$$

where σ ($= 0.8$) is the standard deviation of a 2D Gaussian window w_{ij}. By equalizing contributions of subkernels and using the weight w_{ij}, which is maximum at the center of the original kernel, the influences of the peculiar strong echo can be suppressed and the displacement of the point of interest (center of the original kernel) can be estimated.

In Fig. 1(a), relative positions of kernels $\mathbf{p}_1$ and $\mathbf{p}_2$ in two consecutive frames are illustrated at a certain lag $\delta\mathbf{p} = (\delta\theta, \delta z)$. The position of the kernel in the post frame is defined as $\mathbf{p}_2 = \mathbf{p}_1 + \delta\mathbf{p}$. The size of the search region (range of lag) was set at (0.750°, 0.51 mm) in the lateral and axial directions in the first step, which was larger than the displacement of the heart wall in two frames of 0.125 mm (corresponding to the maximum myocardial velocity of 90 mm/s at a frame rate of 720 Hz[41]). The coarse displacement (u_θ, u_z) was determined from the lag $(\widehat{\delta\theta}, \widehat{\delta z})$, which maximizes the total correlation function $\gamma(\delta\theta, \delta z)$.

2.2 Second step: Fine displacement estimation using smaller kernel

In the second step, a smaller kernel is used to estimate the fine displacement of the point of interest because a smaller kernel is less affected by myocardial deformation. However, there might be multiple regions having echo patterns similar to that in a smaller kernel.[42,43] Therefore, as shown in Fig. 1(b), a search region (0.375°, 0.05 mm) in the lateral and axial directions, which is smaller than that used in the first step, is assigned around the position $\mathbf{p}_1$, and the residual displacement is finely estimated by conventional speckle tracking with a smaller kernel in the lateral and axial directions. The size of the search region (0.375°, 0.05 mm) corresponded to the lateral and axial intervals of the sampled RF signals because displacement larger than the sampling interval was compensated in the first step.

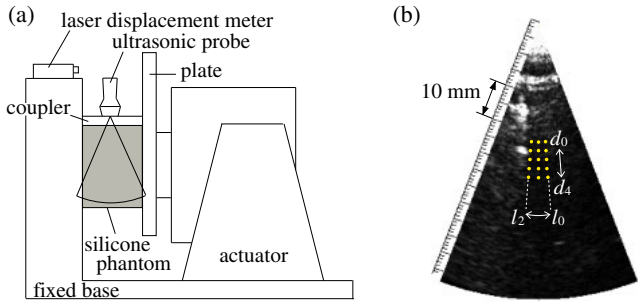

Fig. 2. (Color online) (a) Schematic of experiment using silicone phantom. (b) Points of interest for displacement estimation overlaid on B-mode image of phantom.

3. Basic experiment

3.1 Basic experimental setup

The proposed two-step tracking method was validated by a basic experiment using a phantom ($60 \times 80 \times 80\,\text{mm}^3$) made of urethane rubber. The phantom contains 1% carbon powder by weight to induce sufficient scattering from the inside of the phantom. As shown in Fig. 2(a), the phantom was attached to a fixed base and the phantom was deformed by an actuator. The frequency of sinusoidal motion of the actuator was set at 8 Hz. The displacement of points of interest (l_i, d_j) $(i = 0, 1, 2; j = 0, 1, \ldots, 4)$ inside the phantom shown in Fig. 2(b) were estimated by the proposed method and the conventional method, and the accuracy of each method was evaluated. The displacement of the plate attached to the actuator was measured using a laser displacement meter (Keyence LK-G155) to obtain the spatial distribution of true displacements in the phantom.

The spatial distribution of true displacements was obtained by the finite-element method (FEM)[44] using the displacement of the plate measured using laser. The FEM analysis was performed with a commercial software (Hokuto FEMLEEG version 4.2). By FEM analysis, the amplitude of displacement $A(l)$ at each horizontal position l in the phantom can be estimated as shown in Fig. 3(b). In the present study, the magnitude of displacement applied to an edge ($l = 60\,\text{mm}$) of the phantom (corresponding to the vibrating plate) was set at 1 mm in the FEM analysis. Using amplitude $A(l)$ estimated by the FEM, the true displacement $x_0(l; n)$ at the horizontal position l in the n-th frame is obtained as follows:

$$x_0(l; n) = x_{\text{laser}}(n) \cdot \frac{A(l)}{A(l = 60\,\text{mm})}, \quad (3)$$

where $x_{\text{laser}}(n)$ is the displacement of the vibrating plate measured using laser.

For evaluation of the accuracy, the root mean square error (RMSE) ε was calculated using the true displacement $x_0(l; n)$ and the estimated displacement $x(l, d; n)$ at horizontal and vertical positions l and d as follows:

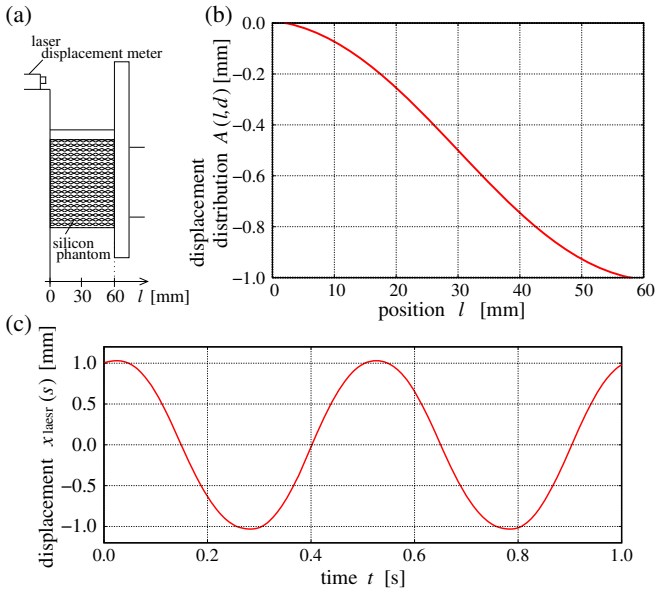

Fig. 3. (Color online) (a) Illustration of laser measurement of plate vibrated by actuator. (b) Distribution of amplitude of displacements estimated by finite-element method. (c) Displacement of plate attached to actuator measured by laser displacement meter.

$$\epsilon = \sqrt{\frac{1}{M \cdot N} \sum_{j=0}^{4} \sum_{i=0}^{4} \sum_{n=0}^{N-1} \{x_0(l_i; n) - x(l_i, d_j; n)\}}, \quad (4)$$

where N and M $(= 25)$ are the numbers of frames and measurement points used in the calculation of RMSE, and (l_i, d_j) are horizontal and vertical positions of each measurement point.

Ultrasonic RF echoes were acquired using a modified ultrasound system (Hitachi-Aloka α-10) with a 3.75 MHz phased array probe. Through the use of parallel receive beamforming (PBF) with plane wave transmissions,[45,46] the frame rate of 720 Hz was realized. The maximum motion velocity of the plate attached to the actuator was about 10 mm/s, which was much smaller than a typical motion velocity of the heart wall of 50 mm/s.[47–49] Therefore, the interval in the calculation of the cross-correlation function was set at 5 frames so that the displacement between two frames became similar to that of the heart wall.[41,42] The lateral and axial spacing of the acquired RF data were 0.375° and 51.3 µm (corresponding to a sampling frequency of 15 MHz), respectively. The myocardial displacement between two consecutive frames is approximately 70 µm under a typical myocardial velocity of 50 mm/s and frame rate of 720 Hz. To accurately estimate such a small displacement, the cross-correlation function was interpolated by a factor of $(120, 50)$ in the lateral and axial directions by reconstructive interpolation[50] to improve the resolution in the estimation of the displacement. The spacing of the cross-correlation function after interpolation was $[3.1 \times 10^{-3}$ deg (0.2 µm at depth 40 mm), 1.0 µm] in the lateral and axial directions.

As shown in Fig. 4, the size of a correlation kernel in the lateral and axial directions (W_l, W_d) were defined on the basis of the size of the point spread function (PSF) of (lateral, axial) $= (\Delta l, \Delta d)$.[41] The size of the correlation kernel $(W_l \times W_d)$ was defined as

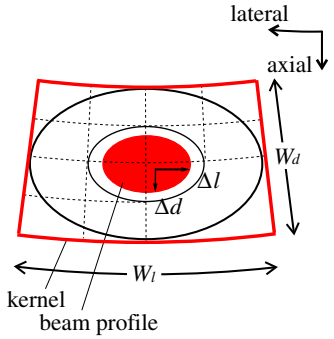

Fig. 4. (Color online) Schematic of correlation kernel.

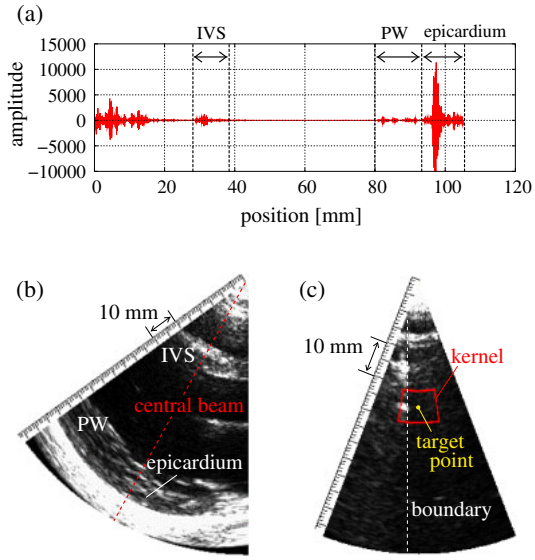

Fig. 5. (Color online) (a) RF signal and (b) B-mode image of human heart which contains strong reflector, i.e., epicardium. (c) Correlation kernel and boundary indicated on B-mode image of phantom.

$$(W_l \times W_d) = \pm 2(\alpha_l \cdot \Delta l \times \alpha_d \cdot \Delta d), \quad (5)$$

where α_l and α_d are the variable coefficients. In the first step of the proposed method, (α_l, α_d) were set at $(1.0, 1.0)$ by referring to our previous study.[41] In the second step, to examine the appropriate size of a correlation kernel, RMSEs were evaluated at various values of α_d from 0.1 to 0.8. The lateral width of a correlation kernel α_l was set at 1.0 because the lateral size of the PSF is larger than the axial size and there was no oscillation, such as that owing to the ultrasonic frequency in the axial direction, in the lateral direction. The size of the PSF $(\Delta l, \Delta d)$ was $(2.40, 2.28)$ mm. In the conventional speckle tracking method, the correlation kernel size was the same as that of the proposed method in the first step.

Furthermore, in the actual in vivo measurement of the heart, amplitudes of echoes from strong scatterers, such as the epicardium, are much higher than those from the myocardium, as shown in Figs. 5(a) and 5(b). To simulate the existence of such strong echoes, a custom-made phantom (containing 1% graphite powder by weight), shown in Fig. 5(c), was used. The phantom had a boundary, and the boundary generates stronger echoes than those from inside the phantom.

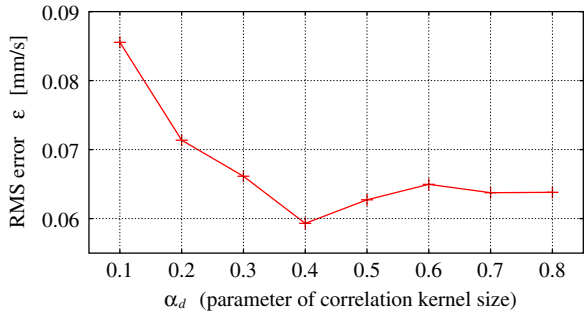

Fig. 6. (Color online) RMSE ϵ obtained for each parameter of the correlation kernel size in axial direction α_d.

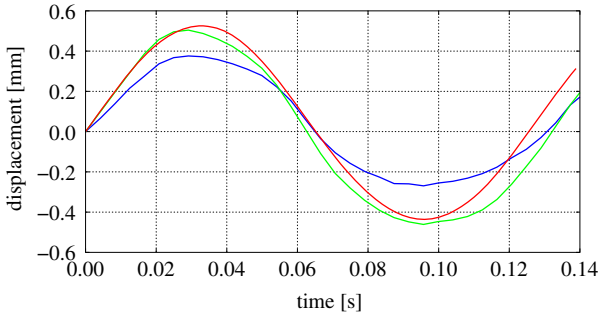

Fig. 7. (Color online) True displacement (red) and estimated displacements (blue: conventional, green: proposed) at point (l_1, d_2) when using proposed method and conventional method.

3.2 Experimental results

Figure 6 shows RMSEs obtained at different $\{\alpha_d\}$ by the proposed method. RMSE was minimum when α_d was 0.4. Therefore, the displacement estimated by the proposed method at $\alpha_d = 0.4$ [correlation kernel size was (13.8°, 3.6 mm)] was compared with the displacement estimated by the conventional method. Figure 7 shows examples of displacement waveforms at point (l_1, d_2) obtained by the FEM analysis, proposed method, and conventional speckle tracking method. In the conventional speckle tracking method, the correlation function was interpolated by a factor of $(120, 50)$, which was the same as that in the second step of the proposed method. As shown in Fig. 7, the displacement estimated by the proposed method is much closer to the true displacement, compared with that estimated by the conventional method. By estimating displacements at each of 15 measurement points, RMSE ε values obtained by the proposed and conventional methods were 0.059 and 0.097 mm, respectively. It was confirmed that RMSE was reduced by 39.2% when using the proposed two-step tracking method. However, the standard variations of RMSE obtained by the proposed and conventional methods were 0.025 and 0.010 mm, respectively. The displacement estimation by the proposed method was more accurate but less stable. In this experiment, amplitudes of the boundary at the edge of the kernels were high, and the displacement estimated from the kernel became similar to the displacement around the edge of the kernel, which was different from the displacement at the center of the kernel (= point of interest).

Figure 8(a) shows correlation coefficients $\{\gamma_{ij}(\delta\theta, \delta z)\}$ obtained from the respective subkernels when the total correlation function $\gamma(\delta\mathbf{p})$ is maximum. By equalizing the contribution of subkernels and applying the highest weight to the central subkernel, the correlation coefficient in the central subkernel became the highest when the total correlation function was maximum, as shown in Fig. 8(a). Also, the correlation coefficient in the second step was, in total, higher than that obtained by the conventional method because a smaller kernel was less influenced by the myocardial deformation and obtained a better match between echo patterns in two frames.

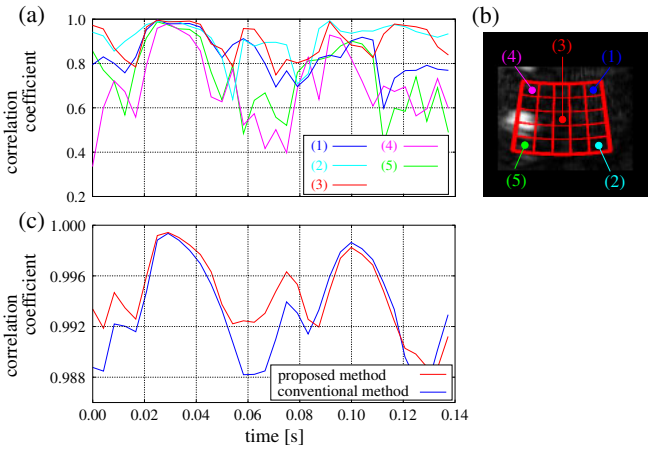

Fig. 8. (Color online) (a) Correlation coefficients obtained from subkernels at maximum of total correlation function. (b) Assigned correlation kernel and subkernels overlaid on B-mode image of phantom. (c) Maximum correlation coefficients obtained by the conventional and second step of the proposed method.

It is difficult to estimate the displacement of a point of interest (the central point of the entire kernel in the first step) when the subkernel is large and a strong scatterer, which is distant from the point of interest, is included in the central subkernel, because the maximum distance between the strong scatterer and the point of interest depends on the size of the subkernel. A larger distance between a point of interest and a strong scatterer would leads to a larger error in the estimation of the displacement of the point of interest because the estimated displacement is significantly influenced by the strong scatterer and the displacement of the strong scatterer is different from the displacement of a scatterer at the point of interest. Therefore, smaller subkernels are desirable. However, the uniqueness of the echo pattern in a subkernel is degraded and the accuracy in the displacement estimation would be degraded when subkernels are too small. In the present study, RMSEs of the estimated displacements were evaluated for various numbers of divisions of the kernel in the first step. As shown in Fig. 9, RMSE tends to increase on increasing the number of divisions. In the present study, five divisions were employed because RMSE increases significantly between 5 and 6 divisions.

Furthermore, to examine the appropriate weight function w_{ij}, RMSEs of the estimated displacements were also evaluated under the various values of the standard deviation σ of the Gaussian distribution. In Fig. 10, RMSE almost converges to 0.055 mm at $\sigma = 0.8$. A smaller σ corresponded to a smaller effective size of a kernel, and RMSE was larger when using a smaller kernel. However, a kernel is desired to be as small as possible for a better spatial resolution in the

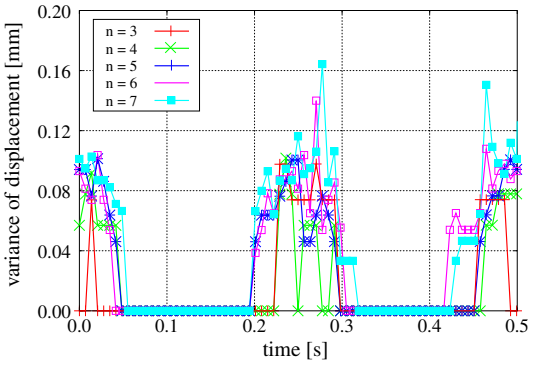

Fig. 9. (Color online) Variance of estimated displacement in lateral direction at point (l_2, d_2).

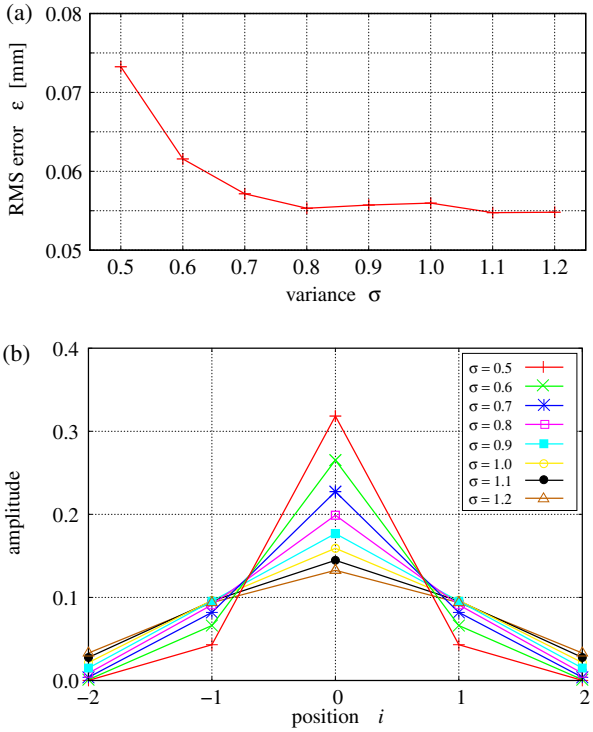

Fig. 10. (Color online) (a) RMSE obtained by each variance σ. (b) Weight function w_{ij} $(j = 0)$.

displacement estimation. Therefore, in the present study, $\sigma = 0.8$ was used.

4. In vivo measurement of human heart

Figure 11(b) shows a B-mode image of the heart obtained from a healthy 22-year-old male. The ultrasonic data were acquired in the long-axis view of the left ventricle, as illustrated in Fig. 11(a). The ultrasonic data were composed of 144 scan lines at lateral intervals of 0.375°, and the frame rate was 560 Hz. The kernel size used for the first and second steps were (13.5°, 13.2 mm) and (6.8°, 6.6 mm), respectively. As in the basic experiment, the correlation kernel size was determined by PSF $(\Delta l, \Delta d) = (3.68, 2.35)$ mm and $(\alpha_l, \alpha_d) = (1.0, 0.4)$. The sizes of search regions were the same as those used in the basic experiment. The instantaneous motion velocity at a point assigned in the posterior wall (PW) of the left ventricle was estimated by the proposed and conventional methods.

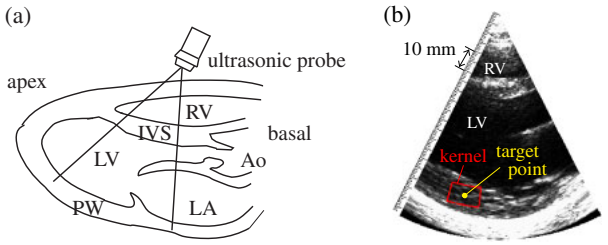

Fig. 11. (Color online) (a) Illustration of acquisition area of RF echo signals in long-axis view of left ventricle. (b) Velocity is estimated at the yellow point displayed on B-mode image.

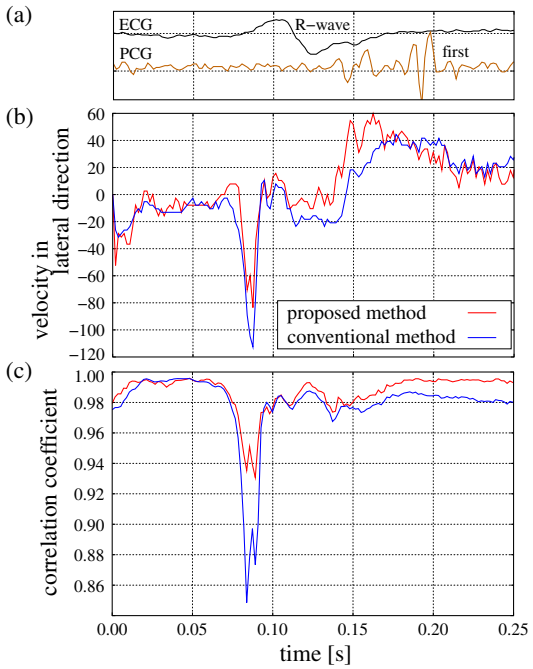

Fig. 12. (Color online) In vivo experimental results. (a) Electrocardiogram and phonocardiogram. (b) Estimated velocities. (c) Maximum correlation coefficients.

Figure 12(a) shows the electrocardiogram (ECG) and phonocardiogram (PCG). Figures 12(b) and 12(c) show the estimated velocities in the lateral direction of the PW around the R-wave and the estimated maximum correlation coefficients. The red and blue lines indicate the results obtained by the proposed and conventional methods, respectively. In the period from 0.07 to 0.10 s, the correlation coefficient is significantly decreased, presumably by the myocardial deformation. During that period, a more deviant velocity was found in the velocity waveform estimated by the conventional method. With the proposed method, the correlation coefficient was significantly increased, and the deviation in the estimated velocity was suppressed.

Figure 13 shows RF signals obtained along two scan lines in the correlation kernels. The time shifts between RF signals shown in Figs. 13(1) and 13(2) were compensated by the proposed and conventional methods. Figures 13(a) and 13(b) show RF signals in the scan lines at the center and edge of the kernel. RF signals in the 46th and 47th frames (significant decrease in the correlation coefficient was observed in these

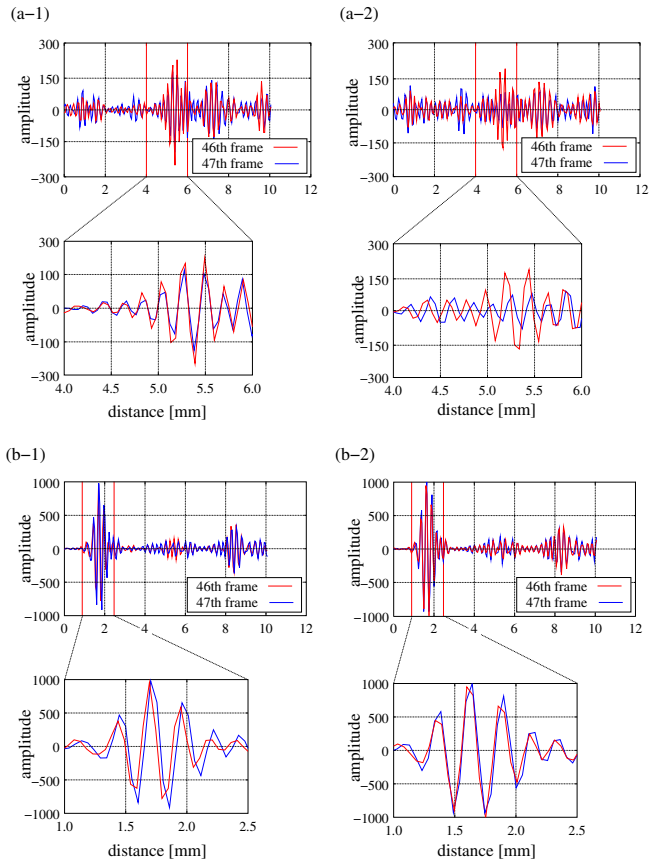

Fig. 13. (Color online) RF signals in scan lines at the center (a) and edge (b) of kernel. RF signals were analyzed by proposed method (1) and conventional method (2).

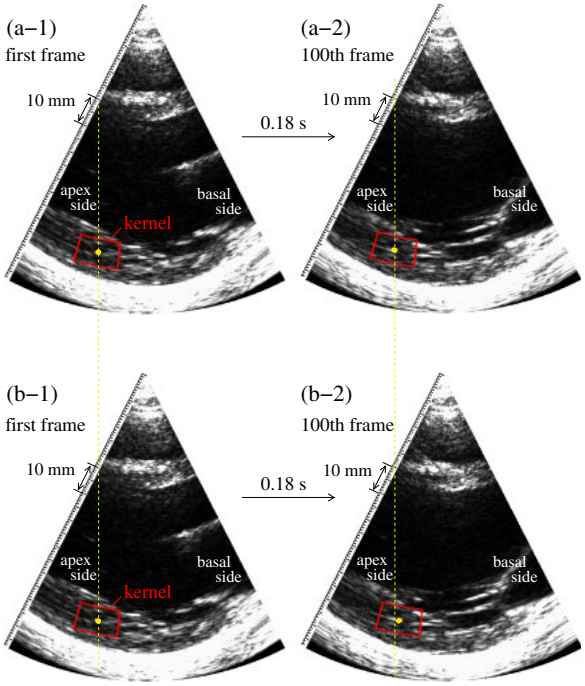

Fig. 14. (Color online) Position of interest and correlation kernel obtained by (a) proposed method and (b) conventional method. (1) First frame in analysis period. (2) 100th frame.

frames) are presented. In this case, the amplitudes of echoes in the scan line at the edge [Fig. 13(b)] are significantly higher than those in the central scan line. Therefore, in the conventional method, RF signals in the scan line at the edge match better than those in the central scan line and, thus, the displacement of the point of interest (center of the kernel) cannot be estimated correctly. On the other hand, in the proposed method, RF signals in the central scan line match better than those in the scan line at the edge, and the displacement at the point of interest can be estimated.

Furthermore, the improvement in displacement estimation was also evaluated by visual inspection of the motion of the point of interest. In Fig. 14, the positions of the point of interest in the first and 100th frames are shown on the corresponding B-mode images. The sector drawn in red indicates the correlation kernel, and its movement represents the estimated displacement of the heart wall between 100 frames. The first frame corresponds to 0 s, and the 100th frame is at approximately 0.18 s in Fig. 12. In the result obtained by the conventional method, shown in Fig. 14(b), there is an erroneous movement of the point of interest toward the base of the heart, although the corresponding movement was not seen by visual inspection because strong echoes in the base side, which moved to the base side, were included in the correlation kernel. In the results obtained by the proposed method [Fig. 14(a)], such erroneous movement did not arise owing to the suppression of the contributions of such strong echoes.

5. Conclusions

In the present study, we proposed a two-step tracking method to estimate the displacement of a deforming object, such as the heart wall. We conducted an experiment using a silicone phantom to evaluate the accuracy of our proposed method. The RMSE obtained by the proposed method was smaller than that obtained by the conventional method. Furthermore, the proposed method was applied to in vivo measurement of the human heart, and the erroneous velocity estimation was suppressed when using the proposed method. These results show the potential of the proposed method for more accurate measurement of the cardiac function.

1) D. H. O'Leary, J. F. Polak, R. A. Kronmal, T. A. Manolio, G. L. Burke, and S. K. Wolfson, New Engl. J. Med. **340**, 14 (1999).
2) M. L. Bots, A. Hofman, P. T. V. M. D. Jong, and D. E. Grobbee, Ann. Epidemiol. **6**, 147 (1996).
3) D. Baldassarre, M. Amato, A. Bondioli, C. R. Sirtori, and E. Tremoli, Stroke **31**, 2426 (2000).
4) S. M. Ellis, R. P. Naoumova, C. K. Neuwirth, R. Eckersley, D. O. Cosgrove, G. R. Thompson, and P. S. Sidhu, Ultrasound Med. Biol. **33**, 1029 (2007).
5) I. M. Graf, F. H. B. M. Schreuder, J. M. Hameleers, W. H. Mess, R. S. Reneman, and A. P. G. Hoeks, Ultrasound Med. Biol. **35**, 955 (2009).
6) P. H. Davis, J. D. Dawson, M. B. Blecha, R. K. Masterbergen, and M. Sonka, Ultrasound Med. Biol. **36**, 560 (2010).
7) S. Kageyama, H. Hasegawa, and H. Kanai, Jpn. J. Appl. Phys. **52**, 07HF04 (2013).
8) N. Ibrahim, H. Hasegawa, and H. Kanai, Jpn. J. Appl. Phys. **52**, 07HF03 (2013).
9) N. Ibrahim, H. Hasegawa, and H. Kanai, Jpn. J. Appl. Phys. **51**, 07GF07 (2012).
10) K. Kitamura, H. Hasegawa, and H. Kanai, Jpn. J. Appl. Phys. **51**, 07GF08 (2012).
11) R. Suresh, M. Grogan, J. J. Maleszewski, P. A. Pellikka, M. Hanna, A. Dispenzieri, and N. L. Pereira, J. Am. Soc. Echocardiogr. **27**, 440 (2014).
12) S. Kutty, T. M. Colen, and J. F. Smallhorn, J. Am. Soc. Echocardiogr. **27**,

155 (2014).
13) D. H. Wiener, J. Am. Soc. Echocardiogr. **27**, 1 (2014).
14) H. Takahashi, H. Hasegawa, and H. Kanai, Jpn. J. Appl. Phys. **52**, 07HF17 (2013).
15) H. Takahashi, H. Hasegawa, and H. Kanai, Jpn. J. Appl. Phys. **50**, 07HF16 (2011).
16) M. M. Nillesen, R. G. P. Lopata, H. J. Huisman, J. M. Thijssen, L. Kapusta, and C. L. de Korte, Ultrasound Med. Biol. **37**, 1409 (2011).
17) K. Ikeshita, H. Hasegawa, and H. Kanai, Jpn. J. Appl. Phys. **51**, 07GF14 (2012).
18) H. Hasegawa and H. Kanai, IEEE Trans. Ultrason. Ferroelectr. Freq. Control **55**, 1921 (2008).
19) H. Kanai, H. Hasegawa, M. Ichiki, F. Tezuka, and Y. Koiwa, Circulation **107**, 3018 (2003).
20) C. L. de Korte, M. Sierevogel, F. Mastik, C. Strijder, J. A. Schaar, E. Velema, G. Pasterkamp, P. W. Serruys, and A. F. W. van der Steen, Circulation **105**, 1627 (2002).
21) H. Shida, H. Hasegawa, and H. Kanai, Jpn. J. Appl. Phys. **51**, 07GF05 (2012).
22) G. R. Sutherland, G. D. Salvo, P. Claus, J. D'hooge, and B. Bijnens, J. Am. Soc. Echocardiogr. **17**, 788 (2004).
23) A. Heimdal, A. Støylen, H. Torp, and T. Skjærpe, J. Am. Soc. Echocardiogr. **11**, 1013 (1998).
24) H. Kanai, H. Hasegawa, N. Chubachi, Y. Koiwa, and M. Yanaka, IEEE Trans. Ultrason. Ferroelectr. Freq. Control **44**, 752 (1997).
25) J. D'hooge, B. Bijnens, J. Thoen, F. van de Werf, G. R. Sutherland, and P. Suetens, IEEE Trans. Med. Imaging **21**, 1022 (2002).
26) H. Yoshiara, H. Hasegawa, H. Kanai, and M. Tanaka, Jpn. J. Appl. Phys. **46**, 4889 (2007).
27) H. Kanai, IEEE Trans. Ultrason. Ferroelectr. Freq. Control **52**, 1931 (2005).
28) S. Langeland, J. D'hooge, H. Torp, B. Bijnens, and P. Suetens, Ultrasound Med. Biol. **29**, 1177 (2003).
29) L. N. Bohs, B. J. Geiman, M. E. Anderson, S. C. Gebhart, and G. E. Trahey, Ultrasonics **38**, 369 (2000).
30) S. Langeland, J. D'hooge, T. Claessens, P. Claus, P. Verdonck, P. Suetens, G. R. Sutherland, and B. Bijnens, IEEE Trans. Ultrason. Ferroelectr. Freq. Control **51**, 1537 (2004).
31) H. Geyer, G. Caracciolo, H. Abe, S. Wilandsky, S. Carerj, F. Gentile, H. J. Nesser, B. Khandheria, J. Narula, and P. P. Sengupta, J. Am. Soc. Echocardiogr. **23**, 351 (2010).
32) J. D'hooge, E. Konofagou, F. Jamal, A. Heimdal, L. Barrios, B. Bijnens, J. Thoen, F. Van de Werf, G. Sutherland, and P. Suetens, IEEE Trans. Ultrason. Ferroelectr. Freq. Control **49**, 281 (2002).
33) F. Yeung, S. Thphen, F. Levinson, and K. J. Parker, Ultrasound Med. Biol. **24**, 427 (1998).
34) J. Jiang and T. J. Hall, IEEE Trans. Ultrason. Ferroelectr. Freq. Control **58**, 730 (2011).
35) T. G. Fisher, T. J. Hall, S. Pamda, M. S. Richaeds, P. E. Barbone, J. Jiang, J. Resnick, and S. Barnes, Ultrasound Med. Biol. **36**, 978 (2010).
36) J. Jiang and T. J. Hall, IEEE Trans. Ultrason. Ferroelectr. Freq. Control **53**, 1088 (2006).
37) A. J. Viterbi, IEEE Trans. Inf. Theory **13**, 260 (1967).
38) Y. Zhu, T. J. Hall, and J. Jiang, IEEE Trans. Med. Imaging **22**, 890 (2003).
39) B. S. Ramamurthy and G. E. Trahey, Ultrason. Imaging **13**, 252 (1991).
40) D. Rappaport, D. Adam, P. Lysyansky, and S. Riesner, Ultrasound Med. Biol. **32**, 1181 (2006).
41) Y. Honjo, H. Hasegawa, and H. Kanai, Jpn. J. Appl. Phys. **51**, 07GF06 (2012).
42) Y. Honjo, H. Hasegawa, and H. Kanai, Jpn. J. Appl. Phys. **49**, 07HF14 (2010).
43) W. Walker and G. E. Trahey, IEEE Trans. Ultrason. Ferroelectr. Freq. Control **42**, 301 (1995).
44) J.-C. Hsu and T.-T. Wu, Jpn. J. Appl. Phys. **49**, 07HB11 (2010).
45) H. Hasegawa and H. Kanai, IEEE Trans. Ultrason. Ferroelectr. Freq. Control **55**, 2626 (2008).
46) D. P. Shattuck, M. D. Weinshenker, S. W. Smith, and O. T. von Ramm, J. Acoust. Soc. Am. **75**, 1273 (1984).
47) H. Kanai, H. Hasegawa, and K. Imamura, Jpn. J. Appl. Phys. **45**, 4718 (2006).
48) H. Kanai, M. Sato, Y. Koiwa, and N. Chubachi, IEEE Trans. Ultrason. Ferroelectr. Freq. Control **43**, 791 (1996).
49) H. Kanai and M. Tanaka, Jpn. J. Appl. Phys. **50**, 07HA01 (2011).
50) I. Cespedes, Y. Huang, J. Ophir, and S. Spratt, Ultrason. Imaging **17**, 142 (1995).